Macromolecules

Article

pubs.acs.org/Macromolecules

Carboxyl-Terminated Polybutadiene–Poly(styrene-*co*-4-vinylpyridine) Supramolecular Thermoplastic Elastomers and Their Shape Memory Behavior

Fang Xie,[†,‡] Chongwen Huang,[‡] Fei Wang,[‡] Longnan Huang,[§] R. A. Weiss,*[,‡] Jinsong Leng,*[,∥] and Yanju Liu*[,†]

[†]Department of Astronautical Science and Mechanics, Harbin Institute of Technology, Harbin 150001, China

[‡]Department of Polymer Engineering, The University of Akron, Akron, Ohio 44325, United States

[§]Department of Materials Science and Engineering, Harbin Institute of Technology at Weihai, Weihai 264209, China

[∥]Center for Composite Materials and Structures, Harbin Institute of Technology, Harbin 150080, China

ABSTRACT: Aiming at an easy-processing metallo-supramolecular polymer which possesses the shape memory property and large deformation ability, we designed a simple metal coordination complex: the blends of zinc-neutralized carboxyl-terminated polybutadiene and poly(styrene-*co*-4-vinylpyridine) (PSVP). The two polymers are tightly bound due to the metal coordination interactions between Zn^{2+} ions from carboxyl-terminated polybutadiene and the pyridine group of the PSVP. The elastomer had reasonably good mechanical properties and was thermoplastic. Improvements in mechanical properties of the blends were realized in the rheology analysis compared with a blend without the introduction of the zinc salt. Small-angle X-ray scattering characterization showed that the microstructure of the elastomeric blend consisted of microphase-separated glassy nanodomains of principally PSVP, which served as cross-link junctions that were connected with polybutadiene chains. The elastomer exhibited good shape memory properties for large deformations, and its shape recovery efficiency could reach 81% in the first cycle and could reach 97% ± 1% in the following seven cycles.

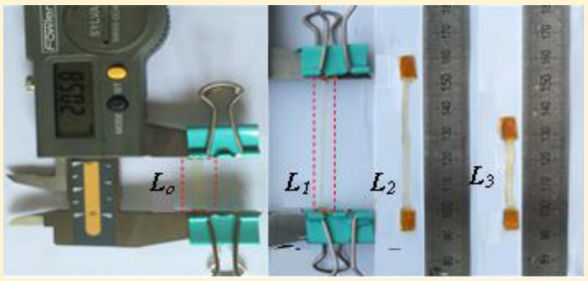

INTRODUCTION

A shape memory polymer (SMP) is a smart polymeric material that can recover its original shape from a temporary shape when exposed to an external stimulus.[1−3] Thermal responsive SMPs have a permanent shape but can be programmed into a temporary shape above a critical, switching temperature (T_c), which can be fixed and stored below T_c and later be converted back to the permanent shape when reheated above T_c. Compared with shape memory alloys, SMPs have the advantages of light weight, low cost, simple processing technology, large deformation, biodegradability, and biocompatibility. Example applications include heat shrinkable tubes,[4] smart textiles,[5] medical devices and auxiliary equipment,[6] color changing materials,[7] information carrier,[8] smart mandrels,[9] and deployable space structures.[10−12]

For the majority of SMPs, T_c is based on the glass transition or a melting transition, but other chemistries, such as reversible Diels–Alder reactions,[13,14] and supramolecular bonds, such as hydrogen bonds,[15,16] ionic interactions,[17−19] and hydrophobic interactions,[20] have more recently received attention. Metal coordination interactions have been used to design functional soft materials,[21,22] including SMPs.[23,24] For example, the lone pair of electrons on the nitrogen atom in pyridine occupy an extra sp^2 hybrid orbital that does not participate in electron delocalization within the aromatic ring. This free electron pair makes pyridine weakly alkaline, which promotes bond interactions via an electrophilic attack. Thus, pyridine and its derivatives are widely used as a ligand in coordination chemistry.[25−27] Kumpfer and Rowan[23] synthesized SMP films using covalently cross-linked metallo-supramolecular polymers based on low molecular weight poly(butadiene) end-capped with 4-oxy-2,6-bis(*N*-methylbenzimidazolyl)pyridine that forms a high molecular weight supramolecular polymer when complexed with a metal salt. Similarly, Xia et al.[24] reported a metallo-supramolecular SMP composed of poly(*n*-butyl acrylate-*co*-methyl methacrylate) with 2,6-bis(1′-methylbenzimidazolyl)pyridine side groups cross-linked by a zinc salt. A shortcoming of the prior work on SMPs based on pyridine–salt complexes is that the synthetic procedures were fairly complicated.

The objective of the work reported herein was to design a metallo-supramolecular SMP by a facile process using polymer blends synthesized by simple chemical syntheses. Specifically, a metal coordination complex was used that involved a blend of zinc-neutralized carboxyl-terminated polybutadiene (CTB) with poly(styrene-*co*-4-vinylpyridine) (PSVP). Similar polystyr-

Received: August 17, 2016
Revised: September 15, 2016
Published: September 22, 2016

DOI: 10.1021/acs.macromol.6b01785
Macromolecules 2016, 49, 7322−7330

ene/polydiene elastomer blends with transition-metal or ionic interactions have been previously studied,[28−31] though not as shape memory materials. Weiss and Sasongko[28] studied graft copolymers produced from ionic interactions or transition-metal complexation between the zinc salt of sulfonated polystyrene and amine-terminated polyisoprene. Zhang et al.[29] prepared a multiblock copolymer using proton transfer between telechelic oligomers, an amine-terminated liquid polyisobutylene, and a telechelic sulfonated polystyrene. Sen et al.[30,31] reported the synthesis of supramolecular networks formed by transition metal coordination of PSVP with 3.4 mol % of VP and the copper salt of a carboxylate-terminated polybutadiene (Cu-CTB). The two polymer components exhibited microphase separation that was stabilized by the Cu-VP complex. Zhao et al.[32] studied mixtures of carboxyl-terminated PS with poly(4-vinylpyridine), P4VP, in solution and reported the formation of micelle-like clusters with a PS-rich core and P4VP corona where P4VP chain bridged two or more neighboring micelles.

This paper addresses the shape behavior of an elastomer based on a similar CTB-PSVP chemistry as that reported by Sen et al.[30,31] In this case, the zinc salt of CTB (Zn-CTB) was used, and the VP content of the PSVP copolymer was much higher than that used by Sen et al.[30,31] The higher VP content of the PSVP allowed for lower PSVP content in the blend so that elastomeric compositions could be achieved. Based on the results in refs 30 and 31, the microstructure of this supramolecular system was of PSVP domains dispersed in a polybutadiene-rich continuous phase. The PSVP domains are physically cross-linked by Zn-CTB chains that form transition metal complexes between VP groups on neighboring PSVP domains. The microstructure envisioned here is similar to that of a block copolymer where physical cross-links between a hard, plastic dispersed phase serve as a permanent network and some transition of the soft, elastomeric phase provides a reversible, temporary network.

EXPERIMENTAL DETAILS

Materials. Carboxyl-terminated polybutadiene (CTB, Hypro 2000×162 CTB; see Figure 1) was supplied by CVC Thermoset Specialties, Emerald Performance Materials, LLC, and had a number-average molecular weight of 4200 g/mol and contained 0.44 mequiv of carboxyl group per gram of the resin. Poly(styrene-*co*-4-vinylpyridine) (PSVP) was purchased from Scientific Polymer Products, Inc. The weight-average molecular weight was 400 000 g/mol, and the VP content was 50 mol % as reported by the vendor. PSVP was a solid powder with a T_g about 130 °C, and CTB was a liquid with a T_g about −77 °C. Toluene, methanol, and zinc acetate dihydrate were purchased from Sigma-Aldrich Co. LLC. All chemicals were used as received.

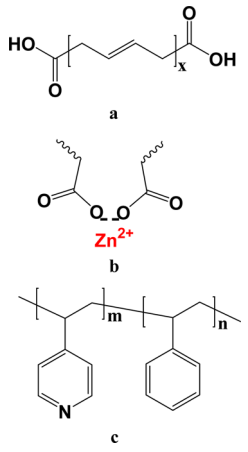

Figure 1. Chemical structures of the component polymers: (a) CTB, (b) ZnCTB, and (c) PSVP.

Sample Preparation. The compositions of all samples are listed in Table 1, and the samples were prepared according to the following procedure. The ZnCTB was prepared by mixing a solution of zinc acetate dihydrate in a 1:1 (v/v) mixture of deionized water and methanol and a solution of CTB in toluene. The stoichiometric ratio of Zn^{2+} and carboxylic acid was 1:2, and the resulting ZnCTB was recovered by evaporating the solvent in air, drying at 50 °C for 24 h, and drying under vacuum at 50 °C for 24 h. Blends of ZnCTB and PSVP were prepared by mixing both components in a common solution of toluene and stirring for 48 h at room temperature. The blend was air-dried at 50 °C for 3 days to remove most of the solvent and then vacuum-dried at 50 °C for 24 h to remove all the solvent. The VP content of the PSVP, 50 mol %, used in this study was much higher than that used by Sen et al.,[30,31] which allowed the use of much lower concentrations of PSVP in the complexes reported herein. The consequence of that difference is that this study focused on elastomeric supramolecular compounds, whereas Sen et al.[30,31] reported plastic compounds. The ZnCTB−PSVP blend formed a transparent and free-standing, flexible elastomer that had a tunable transition temperature between 77 and 121 °C, depending on the composition. Five blends were prepared, which are denoted as ZnCTBPSVP-1:*x* (*x* = 1, 1.5, 2, 4, 8), corresponding to of the ratio of carboxyl groups and pyridine groups of 1:1, 1:1.5, 1:2, 1:4, and 1:8, respectively. A blend of an un-neutralized CTB (i.e., the free-acid derivative) and PSVP was also prepared as a controlled sample, and that sample is referred to as CTBPSVP-1:1.

Table 1. Compositions of the Blend Samples

sample	CTB/PSVP (wt %)	Zn^{2+}/COO^- (mole ratio)	COO^-/VP (mole ratio)	Zn^{2+}/VP (mole ratio)
CTBPSVP-1:1	91.4/8.6	0	0	0
ZnCTBPSVP-1:1	91.4/8.6	1:2	1:1	1:2
ZnCTBPSVP-1:1.5	87.6/12.4	1:2	1:1.5	1:3
ZnCTBPSVP-1:2	81.2/18.8	1:2	1:2	1:4
ZnCTBPSVP-1:4	72.7/27.3	1:2	1:4	1:8
ZnCTBPSVP-1:8	57.1/42.9	1:2	1:8	1:16

Characterization. *FTIR Analysis.* Infrared spectroscopy was used to confirm the metal coordination interactions between the Zn^{2+} ions of ZnCTB and the VP groups of PSVP. The infrared spectra of the copolymers were recorded in transmission mode on a Nicolet AVATAR360 FTIR spectrometer covering a wavelength range of 400−4000 cm^{-1} with a resolution of 2 cm^{-1}. The polymer samples were cast onto KBr wafers, and the solvent was removed under vacuum.

Small-Angle X-ray Scattering (SAXS). The microphase-separated morphology of the blends was confirmed by SAXS using a Rigaku SAXS system equipped with a rotating anode X-ray generator (MicroMax002+) operating at 18 kW and producing Cu Kα (λ = 0.154 nm) radiation. The exposure time for each sample was 300 s. All samples were measured at room temperature.

Thermal Analysis. The thermal properties of the supramolecular elastomer were measured with a TA Instruments DSC Q200 differential scanning calorimetry (DSC) from −90 to 220 °C using a heating and cooling rate of 10 °C min^{-1} and a nitrogen atmosphere. The data reported are from measurements made after first preheating

DOI: 10.1021/acs.macromol.6b01785
Macromolecules 2016, 49, 7322−7330

the samples to 220 °C and then cooling them to −90 °C to eliminate the influence of the prior thermal history.

Rheological and Mechanical Properties. Melt rheology measurements were performed with an Advanced Rheometric Expansion System (ARES) G2 from TA Instruments. A parallel plate fixture with a diameter of 8 mm was used, and the initial thickness of the sample was ∼1 mm. Dynamic frequency sweeps were run at 50 °C covering a frequency (ω) range of 0.0628−628 rad/s, with a strain amplitude (γ) sweep strain of 5%, which was within the linear response region of the samples as determined by a strain sweep. Dynamic mechanical properties of the supramolecular elastomers were measured from −120 to 25 °C with a TA Instruments DMA Q800 in the tension mode with a frequency of 1 Hz, a displacement amplitude of 10 μm, and a heating rate of 3 °C min^{-1}. The specimen was cut to 10 × 5 × 0.5 mm^3 from a compression-molded film. For the temperature range of 25−150 °C, the dynamic mechanical properties were measured in shear with the ARES-G2 rheometer using parallel plates of 8 mm and a frequency of 6.28 rad/s (1 Hz). Static tensile properties were measured with a Zwick/Roell Z010 universal machine using a stretching rate of 10 mm min^{-1} at room temperature.

Shape Memory Behavior. Shape memory properties of elastomer films were measured in tension using a device similar to that reported by Brostowitz et al.[33] that included a vernier caliper and two binder clips to precisely deform a relatively large sample of film in tension. The binder clips were used to fix the sample on the outside jaws of the vernier caliper. A sample with an initial length L_0 was first soaked in hot water (60 °C) and stretched with the vernier caliper to a length of L_1. Note that the use of the water was only heat the sample. The water itself had no influence on the shape memory behavior. The stretched sample was then removed from the water bath and fixed by cooling to room temperature while holding the length constant (i.e., constant strain). The sample fixed in the temporary shape was removed from the caliper and allowed to achieve an equilibrium length of L_2. The recovery efficiency of the SMP was measured by immersing the unloaded sample in its temporary shape into hot water (60 °C) and allowing the sample to recover to length L_3. The shape fixity efficiency, R_f, and shape recovery efficiency, R_r, were defined by eqs 1 and 2, respectively.

$$R_f = \frac{L_2 - L_0}{L_1 - L_0} \times 100\% \quad (1)$$

$$R_r = \frac{L_2 - L_3}{L_2 - L_0} \times 100\% \quad (2)$$

Multiple shape memory cycles for the supramolecular elastomers were performed with the DMA Q800 using a tensile film fixture and the controlled-force mode. For the Nth cycle, the initial strain was ε_{n0}, the stretched strain was ε_{n1}, the fixed strain after cooling and unloading was ε_{n2}, and the recovered strain, which was also the initial strain for the $(N + 1)$th cycle, was $\varepsilon_{(n+1)0}$. The shape fixity efficiency, R_{nf}, and shape recovery efficiency, R_{nr}, of the Nth cycle were calculated using eqs 3 and 4, respectively.

$$R_{nf} = \frac{\varepsilon_{n2} - \varepsilon_{n0}}{\varepsilon_{n1} - \varepsilon_{n0}} \times 100\% \quad (3)$$

$$R_{nr} = \frac{\varepsilon_{n2} - \varepsilon_{(n+1)0}}{\varepsilon_{n2} - \varepsilon_{n0}} \times 100\% \quad (4)$$

RESULTS AND DISCUSSION

Sample Clarity and Formability. Photographs of the solid plastic powder like PSVP, the liquid CTB, and two blend samples, CTBPSVP-1:1 and ZnCTBPSVP-1:1, that were solution cast are shown in Figure 2. The blend CTBPSVP-1:1 (unneutralized CTB mixed with PSVP, Figure 2c) was viscoelastic liquid with a higher viscosity than the neat CTB. It did not hold a shape and could not form a free-standing film. In contrast, the ZnCTBPSVP-1:1 blend of Zn-CTB and PSVP was

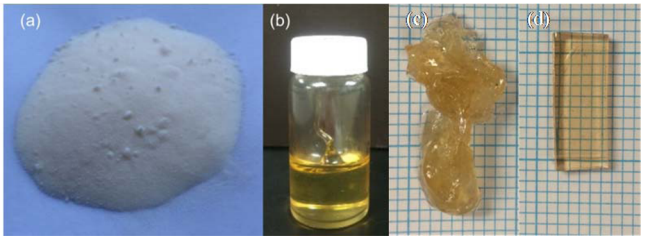

Figure 2. Raw materials and blend samples prepared by solution casting: (a) PSVP, (b) CTB, (c) CTBPSVP-1:1, and (d) ZnCTBPSVP-1:1.

a transparent elastomer and formed a free-standing film at room temperature (Figure 2d). The clarity of the ZnCTBPSVP-1:1 blend is shown in Figure 3a.

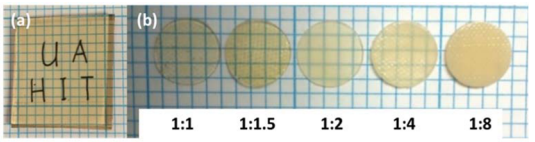

Figure 3. Sample clarity of 0.5 mm thick compression-molded blends: (a) ZnCTBPSVP-1:1; (b) ZnCTBPSVP-1:x (x = 1−8).

All of the ZnCTBPSVP-1:x (x = 1−8) samples formed free-standing flexible elastomeric films (Figure 3b). However, as the concentration of PSVP increased, the samples became turbid, and for the highest PSVP concentration, ZnCTBPSVP-1:8, the sample was opaque. The turbidity and opaqueness of the samples with a Zn-CTB/PSVP ratio of greater than 1:1.5 indicate macrophase separation of the components, since a phase of the order of a micrometer in size is required to scatter light. That does not preclude, however, that there may also be microphase separation in those samples, i.e., a dispersed phase size much smaller than the wavelength of light visible phase separation ≪500 nm, as is discussed later in this paper.

FTIR Analysis. The FTIR spectra of the carboxylic acid-terminated polybutadiene (CTB), its zinc salt (Zn-CTB), and their blends with PSVP are shown in Figure 4. The 1640 cm^{-1}

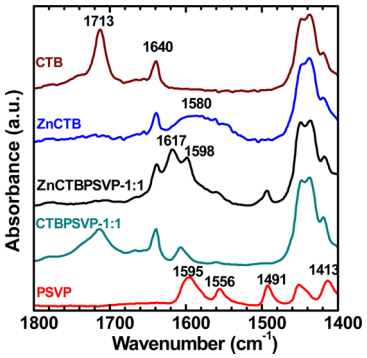

Figure 4. FTIR spectra for component polymers and their blends.

absorption band in all of the samples shown in Figure 4 is due to the C═C stretching vibration of the alkene groups of the polybutadiene. The strong 1713 cm^{-1} and weak 1740 cm^{-1} absorptions for CTB are due to the carbonyl stretching (C═O) of the carboxylic acid group (COOH) in hydrogen-bonded dimers and non-hydrogen-bonded, free carboxylic acid, respectively. Most of the COOH in CTB is present as

DOI: 10.1021/acs.macromol.6b01785
Macromolecules 2016, 49, 7322−7330

hydrogen-bonded dimers. After neutralizing the CTB with zinc acetate, those two absorption bands disappear in favor of a broad absorption at 1580 cm^{-1} that is due to the carbonyl stretching of the carboxylate anion ($-COO^-$). That spectral change provides evidence that the all of the carboxylic acid groups were neutralized to zinc carboxylate.

The carbonyl absorption of CTB broadened considerably for the CTBPSVP-1:1 blend, which can be explained by a variety of environments for the carbonyl groups. In the blend, some hydrogen-bonded COOH dimers are most likely converted to hydrogen-bonded complexes between the hydroxyl group of a COOH and pyridine, the formation of which liberates a free COOH group. An increase of the concentration of free COOH groups would account for the increased absorbance intensity on the higher frequency side of the carbonyl band.

For the spectrum of ZnCTBPSVP-1:1, the broad peak for the carboxylate anion in the Zn-CTB, centered at ~1580 cm^{-1}, disappeared, and two sharper new absorptions occurred at 1617 and 1598 cm^{-1}. Complexation of the zinc cation with the nitrogen of the pyridine group should shift the carbonyl stretching vibration of the carboxylate anion to higher frequency. Thus, either the 1617 cm^{-1} or the 1598 cm^{-1} absorption peak for Zn-CTBPSVP-1:1 may represent a blue-shift of the carbonyl stretching of the Zn-CTB due to the complexation of the zinc ion with the aromatic nitrogen of PSVP. The uncertainty in the band assignment for the Zn-CTB carbonyl peak is that either of those two new absorption peaks for Zn-CTBPSVP-1:1 may also be due to changes in the vibration frequency of the aromatic C−N stretching band. For PSVP, the four absorptions at 1595, 1556, 1491, and 1413 cm^{-1} are due to the aromatic vibrations of the pyridine ring. The absorption at 1595 cm^{-1} is the aromatic C−N stretching band, which is reported to shift to ~1617 cm^{-1} when the nitrogen atom of pyridine ring complexes with a metal ligand in poly(4-vinylpyridine).[27,34,35] Thus, the new absorption at 1617 cm^{-1} for the Zn-CTBPSVP-1:1 blend (Figure 4) is tentatively assigned to a transition metal complex between the zinc cations of Zn-CTB and the nitrogen atoms in PSVP. The 1598 cm^{-1} absorption band, then, is attributed to the blue-shift of the carbonyl stretching vibration of the carboxylate anion.

Note that the hydrogen-bonding energy of the N···H−O and C−H···O hydrogen bonds in this blend system may be as high as 10 kJ/mol.[36] In contrast, the binding energy of a zinc ion and pyridine is over an order of magnitude stronger, ~250 kJ/mol,[37] which explains the differences in the properties of the intermolecular complexes achieved by blending the polymers described herein. Another related, but independent result that indicates strong supramolecular bonding between ZnCTB and PSVP is that the two polymers can be dissolved together in toluene. After solution casting and drying, however, the resulting elastomer film made from ZnCTBPSVP-1:1 did not redissolve in toluene at all. The films made from the blends with higher PSVP had some solubility, which was believed to be the excess PSVP in the sample that was not complexed with the ZnCTB. Those results are consistent with achieving a complex stoichiometric ratio of two pyridine groups to one zinc ion and a supramolecular network formed by those complexes, which were insoluble in toluene.

Thermal Properties. DSC heating thermograms of the samples are shown in Figure 5. The T_gs of PSVP, CTB, and ZnCTB were 130, −77, and −77 °C, respectively. Converting the carboxylic acid groups to zinc carboxylate had no effect on the T_g. The blends exhibited two T_gs: one at about −77 °C that corresponds to a CTB-rich phase and a higher temperature transition that corresponds to a PSVP-rich phase. The higher temperature T_g increased with increasing PSVP concentration.

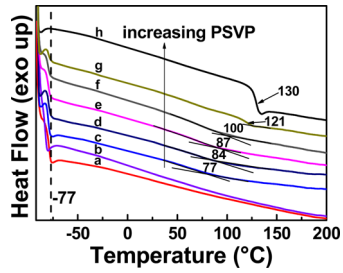

Figure 5. DSC thermograms of component polymers and their blends: (a) CTB, (b) ZnCTB, (c) ZnCTBPSVP-1:1, (d) ZnCTBPSVP-1:1.5, (e) ZnCTBPSVP-1:2, (f) ZnCTBPSVP-1:4, (g) ZnCTBPSVP-1:8, and (h) PSVP.

The insensitivity of the low temperature T_g indicates that the continuous phase of the blend is essentially pure polybutadiene—that is, the PSVP had negligible solubility in the polybutadiene The composition dependent higher temperature T_g suggests that the Zn-CTB may be soluble in the PSVP domains, though it is doubtful that the solubility of Zn-CTB could have been large enough to produce an ~50 °C depression of the PSVP T_g. Alternative explanations for the depression of the PSVP T_g with decreasing PSVP content in the blend are that it was due to the small size and confinement of PSVP nanodomains,[38,39] as was indicated by the SAXS data discussed below, or it was a result of a diffuse interface between the PSVP nanodomains and the continuous polybutadiene phase due to the strong supramolecular bonds, similar to what Robertson et al.[40] reported for poly(isobutylene-*b*-styrene-*b*-isobutylene) block copolymers. The latter explanation is also consistent with the broadening of the PSVP glass transition with decreasing PSVP concentration. The harder PSVP domains act as physical cross-links, similar to the way a hard block acts as a cross-link in elastomeric block copolymers. In this case, however, instead of covalent bonds that connect the soft and hard phases in block copolymers, the connection is a supramolecular bond formed by the ion−metal complex.

SAXS Analysis. Small-angle X-ray scattering (SAXS) measurements of the PSVP, ZnCTB, and ZnCTBPSVP-1:*x* (*x* = 1, 2, 8) blends at room temperature are shown in Figure 6. The scattering pattern of the PSVP was featureless, which was

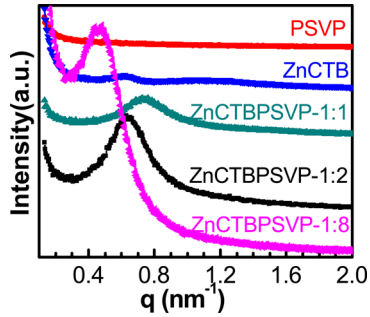

Figure 6. SAXS intensity as a function of scattering vector ($q = 4\pi \sin \theta/\lambda$, where λ is the X-ray wavelength and θ is one-half the scattering angle) for ZnCTB, PSVP, and their blends. The SAXS curves are shifted upward, and each curve was scaled for clarity; i.e., the differences in the scattering intensities of the different curves are not quantitative.

DOI: 10.1021/acs.macromol.6b01785
Macromolecules 2016, 49, 7322−7330

expected from this single phase copolymer. The ZnCTB, however, was microphase-separated, as indicated by a single, broad scattering peak with a maximum intensity at q = 0.62 nm^{-1}, which corresponds to a characteristic spacing, $d = 2\pi/q$, of 10.1 nm. That result is consistent with previous SAXS studies for CTB neutralized with divalent cations reported by Williams et al.,[41] who attributed the correlation to the root-mean-square end-to-end distance of the polybutadiene chains that separate small nanodomains of the metal carboxylate groups.

Figure 6 shows SAXS data for three ZnCTBPSVP, varying in molar ratio of Zn^{2+} to VP from 1:2 to 1:16 (see Table 1). Note that the stoichiometric ratio of Zn^{2+} to VP is 1:2 if all the zinc cations interact with two pyridine groups in the blend. The SAXS pattern for the ZnCTBPSVP-1:1 blend (mass ratio ~91:9) showed a much more prominent scattering peak at q = 0.73 nm^{-1} (d = 8.6 nm) than that in the neat ZnCTB. On the basis of the SAXS results for a similar blend of CuCTB and PSVP with a much lower VP composition[31] and the increase in intensity of the SAXS peak in the blend versus that in the ZnCTB, we do not believe that the SAXS peak in the blend is due to ionic aggregates. The mass composition of the CuCTB/PSVP blend, ~44:56 w/w, which was used in ref 31, was higher than any of the blends used in the present work and corresponds to a sample between curves g and h in Figure 5, though the Cu^{2+}/VP molar ratio was much lower. Still, it is relevant that the SAXS data for that blend indicated that no ionic aggregate structure and the low-q data exhibited a strong upturn in intensity that was distinct from the intensity upturn normally observed for neat ionomers.[31] The loss of the ionic peak in the SAXS for a polymer blend with strong supramolecular interactions involving an ionomer is also consistent with the results reported by Lu and Weiss[42] for blends of a polyamide with sulfonated polystyrene in which an intermolecular transition metal complex formed.

Transmission electron microscopy (TEM) analysis of the CuCTB/PSVP blend in ref 31 showed a bicontinuous microstructure with phase sizes ~100 nm. The SAXS data in that paper were limited to phase sizes less than 10 nm, so the upturn in the SAXS intensity at low q is consistent with a larger phase size, e.g., the ~100 nm scale indicated by TEM. The ZnCTBPSVP-1:1 blend in the present study had a much lower concentration of PSVP than the CuCTB/PSVP blend in ref 31, so it would seem to make sense that if the dispersion of the PSVP was stabilized by complexation with the ZnCTB, the PSVP domains would be much smaller than those in ref 31. That suggests that the d = 8.6 nm size indicated by the SAXS peak in Figure 6 arises from intraparticle scattering from PSVP nanodomains decorated on their surface with zinc ions (see Figure 7). That supposition is supported by the increase in the average PSVP nanodomain size from 8.6, 9.8, and 13.4 nm as the concentration of PSVP increased from a mass ratio of ~91:9 for ZnCTBPSVP-1:1, 81:19 for ZnCTBPSVP-1:2, and 57:43 for ZnCTBPSVP-1:8, respectively. The intensity of the SAXS peak also increased with increasing PSVP concentration.

It should also be noted that the SAXS patterns for the blends also exhibited an intensity upturn at low q that became stronger with increasing PSVP concentration which indicates a correlation length in the structure that may be resolved by light scattering. The SAXS intensity upturn at low q is consistent with the pictures of the sample clarity shown in Figure 3 where the ZnCTBPSVP-1:1 blend was clear, the ZnCTBPSVP-1:2 blend was translucent, and the ZnCTBPSVP-1:8 blend was opaque. The loss of clarity with increasing PSVP concentration is due to macroscopic phase separation, i.e., phase sizes large enough to scatter visible light, >~500 nm, though in addition to the macrophase separation in the turbid and opaque blends, some microphase separation occurs. It is probably not a coincidence that the clearest blend was ZnCTBPSVP-1:1, which possessed a stoichiometric ratio of one zinc ion to two pyridine groups.

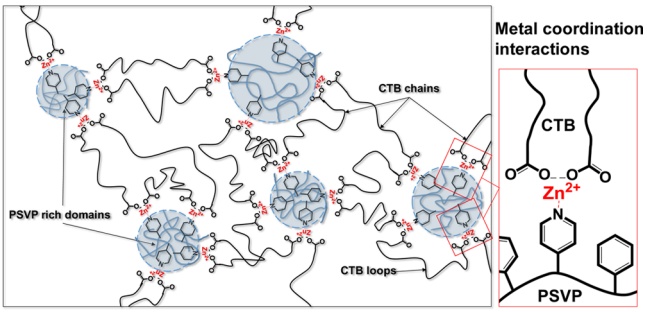

Figure 7. Schematic of the metal coordination interactions in the blend of ZnCTB and PSVP. The PSVP nanodomains are shown as spherical but not necessarily uniform in size. The hypothesis is that ZnCTB chains cross-link PSVP nanodomains by supramolecular bonds between one zinc ion and two pyridine groups. As noted in the schematic, some ZnCTB chains may form loops; i.e., both ends bond with the same PSVP nanodomain. In that case, the CTB chain is ineffective as a network chain.

Oscillatory Rheology Analysis. The frequency dependences of the linear viscoelastic (LVE) properties of CTB, ZnCTB, and the blends at 50 °C are shown in Figure 8. The CTB had negligible elasticity and a frequency-independent viscosity (i.e., it was essentially a Newtonian fluid), so only the loss modulus data, $G''(\omega)$, are plotted in Figure 8 for that sample. For ZnCTB, G'' was greater than the storage modulus, G', and $G' \sim \omega^2$ and $G'' \sim \omega^1$ over the frequency range studied, which is indicative of a nonentangled polymer. However, the dynamic viscosity ($\eta' = G''/\omega$) of ZnCTB, though independent of frequency, was about 6 times that of the parent CTB (η'_{ZnCTB} = 312 Pa·s, η'_{CTB} = 53 Pa·s), which is a consequence of the ionic bonds formed by intermolecular association of the Zn^{2+} cation with two carboxylate groups and intermolecular dipole−dipole associations of the metal carboxylate groups.

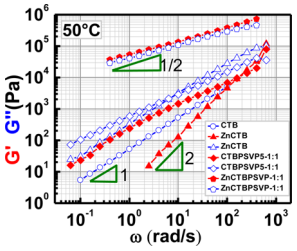

Figure 8. Frequency dependence of the storage modulus, G' (red), and the loss modulus, G'' (blue), at 50 °C for CTB, ZnCTB, and the blends. Strain amplitude = 5%.

The CTBPSVP-1:1 blend was a viscoelastic liquid, i.e., $G'' > G'$, that behaved more like an entangled polymer; i.e., G' and G'' were functions of frequency. The slopes of G' vs ω and G'' vs ω at the lower frequencies were 1 and 0.7, respectively, which indicates that terminal behavior was not achieved for the experiments shown in Figure 8. Note that 50 °C is below the T_g

DOI: 10.1021/acs.macromol.6b01785
Macromolecules 2016, 49, 7322−7330

of the PSVP phase; i.e., the PSVP phase is glassy at this temperature. The zero-shear viscosity, $(G''/\omega)_{\omega\to 0}$, of the blend was about 20 times that of the CTB, and the viscosity of the CTBPSVP-1:1 blend exhibited weak shear thinning at the higher frequencies. The large increase in viscosity was due to the physical cross-links produced by intermolecular hydrogen bonding between the carboxylic acid groups in CTB and the pyridine groups of the PSVP. One might expect that the dispersed glassy PSVP phase may contribute to the viscosity through a filler effect, but that contribution would be relatively small compared to the order of magnitude increase that was observed. For example, an estimation based on the densities of polybutadiene and polystyrene, which give a volume fraction of PSVP of 0.076, and the Einstein equation[43] for the viscosity of a dispersion of solid particles in a liquid accounts for only about 19% of the increase of viscosity observed for the CTBPSVP-1:1 blend.

The elasticity of the CTBPSVP-1:1, as represented by the G' data, was 1−2 orders of magnitude greater than that for ZnCTB. Since the ZnCTB behaved like a Newtonian fluid, a simple filler effect is not expected to account for the large increase of elasticity for CTBPSVP-1:1, but the formation of a hydrogen-bonded polymer−polymer complex does explain the increase of the elasticity. However, the hydrogen-bonding interactions that form the polymer−polymer complex for CTBPSVP-1:1 were much weaker than the intermolecular interactions that occurred in the ZnCTBPSVP-1:1 blend, as was discussed earlier for the FTIR data and is further discussed in the next paragraph.

For the ZnCTBPSVP-1:1 blend $G' \sim G''$ over the entire frequency range, which is indicative of a critical gel.[44] The critical exponent for this system was 0.5, i.e., $G' \sim G'' \sim \omega^{0.5}$. In this system, there were no covalent cross-links, so the network responsible for the liquid to solid transition that occurs at the gel point is due to the intermolecular ion−metal complex between the Zn^{2+} ion and the VP groups. The G' and G'' of ZnCTBPSVP-1:1 were 2 orders of magnitude greater than for the CTBPSVP-1:1. The much higher dynamic modulus (∼100 kPa) for ZnCTBPSVP-1:1, which was comparable to that of a soft rubber, than that for CTBPSVP-1:1 indicates a much higher effective cross-link density, since for a rubber or gel the modulus is proportional to the cross-link density.[45] That result is a consequence of the greater efficiency of forming the Zn^{2+}−pyridine complex than the hydrogen-bonded complex in CTBPSVP-1:1. The lower slope of the G' vs ω curve for ZnCTBPSVP-1:1 compared to CTBPSVP-1:1 also indicates that the strength of the ion−metal supramolecular bond is stronger, that longer relaxation time, than that of the hydrogen bond, which is in accordance with the FTIR results discussed earlier in this paper.

Temperature Dependence of the LVE Properties of ZnCTBPSVP-1:1. The temperature dependence of the dynamic tensile properties at ω = 1 Hz for ZnCTBPSVP-1:1 is shown in Figure 9. The red curve represents the storage modulus function, $E' = E'(\omega = 1, T)$, and the black curve represents the loss modulus, $E'' = E''(1, T)$. The data for T < 25 °C were measured with a DMA using a tensile fixture. For T > 25 °C measurements were made in shear with the ARES rheometer and were converted to tensile properties by multiplying the dynamic and loss shear moduli by a factor of 3, which assumes that the Poisson ratio of the elastomer was 0.5, i.e., that of an incompressible, elastic solid. Note that the

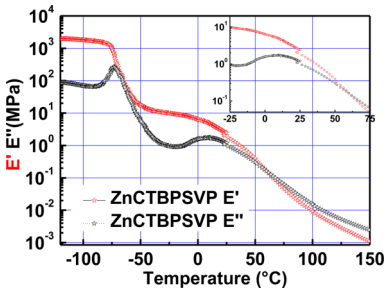

Figure 9. Temperature dependence of the LVE tensile properties for ZnCTBPSVP-1:1 (E', storage modulus (red); E'', loss modulus (black)).

two sets of data shown in Figure 9 superposed very well, which indicates that the latter assumption was reasonable.

The loss modulus curve showed two maxima, at −73 and 11 °C, and the storage modulus decreases coincident with both loss peaks. The lower temperature transition is the glass transition of the continuous CTB phase and agrees with the DSC result reported above. However, the peak position of the higher temperature transition, which represents the glass transition of the PSVP domains, is much lower than that measured by DSC. However, the transition was especially broad, and a crossover temperature where E'' became greater than E' (i.e., a transition from solid-like to liquid-like behavior) was observed at ∼60 °C. The large difference in the determination of the T_g of the PSVP nanodomains is most likely a consequence of the supramolecular nature of the cross-links, so that the effective T_g, or perhaps relaxation behavior is a better descriptor of the domains, is influenced by frequency and the strain amplitude. These data do indicate that with respect to shape memory behavior, it would be advisible to keep the temperature of the system below ∼60 °C, i.e., below the moduli crossover temperature, to maintain a permanent network formed from hard PSVP domains cross-linked by ZnCTB chains. However, the thermoplastic nature of this blend complex, i.e., it undergoes a solid to melt (liquid) transition, is advantageous with regard to melt processing and forming shapes at elevated temperatures.

Tensile Properties. Example tensile stress−elongation curves of ZnCTBPSVP blends at room temperature are shown in Figure 10. Those blends had 100% modulus of ∼0.12−2.1 MPa, tensile strength of ∼0.18−2.2 MPa, ultimate tensile elongation of ∼480−590%, and a strain energy to break (i.e., the area under the curve) of ∼0.82−8.5 MJ/m^3 (see Table 2). It is difficult to make direct comparisons of the mechanical properties of the blend and commercial polybutadiene

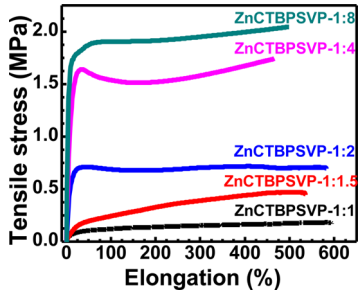

Figure 10. Example tensile stress−elongation curves for ZnCTBPSVP blends.

DOI: 10.1021/acs.macromol.6b01785
Macromolecules 2016, 49, 7322−7330

Table 2. Mechanical Properties of the ZnCTBPSVP Blends

sample	tensile strength (MPa)	100% modulus (MPa)	ultimate tensile elongation (%)	strain energy to break (MJ/m^3)
ZnCTBPSVP-1:1	0.177 ± 0.015	0.121 ± 0.006	571 ± 31	0.82 ± 0.10
ZnCTBPSVP-1:1.5	0.456 ± 0.097	0.251 ± 0.013	530 ± 44	1.9 ± 0.3
ZnCTBPSVP-1:2	0.731 ± 0.138	0.733 ± 0.025	586 ± 63	4.3 ± 0.2
ZnCTBPSVP-1:4	1.67 ± 0.32	1.44 ± 0.27	479 ± 48	6.8 ± 0.5
ZnCTBPSVP-1:8	2.17 ± 0.17	2.05 ± 0.24	501 ± 37	8.5 ± 0.9

compositions because of differences in the butadiene isomer compositions, differences in cross-link density, and the probability of additives in the commercial materials. Typical mechanical properties reported for commercial polybutadiene elastomer are 100% modulus of ∼0.3−3.2 MPa,[46,47] a tensile strength of ∼1−15 MPa,[46−48] and an ultimate elongation of ∼150−1000%.[46,47] The supramolecular complex blends appear to be as stiff as and have the same order of elongation as commercial polybutadiene, but lower tensile strength and lower strain energy to break. However, the mechanical properties are reasonable, especially considering that these blends are predominately composed of a polybutadiene oligomer and there are no covalent cross-links in the system.

Shape Memory Behavior. The shape memory behavior of the elastomer ZnCTBPSVP-1:1 was characterized by a shape memory cycle using a vernier caliper and two binder clip (see Figure 11). The sample with initial length L_0 = 20.6 mm was

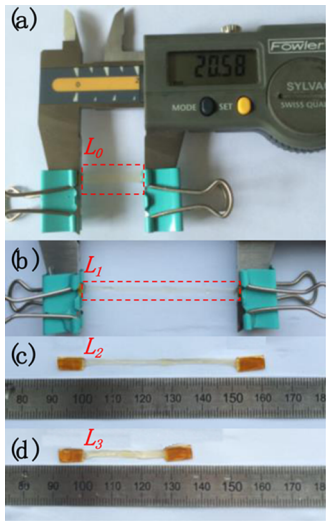

Figure 11. Shape memory process for ZnCTBPSVP-1:1: (a) original shape; (b) stretched temporary shape; (c) unloaded temporary shape; (d) recovered shape.

heated to 60 °C by immersing it in hot water and then stretched to a length of L_1 = 52 mm. The sample stretched, temporary shape was fixed by holding the stretched sample in the caliper and removing it from the hot water and cooling it to room temperature. After unloading the sample from the caliper (i.e., removing the stress holding the sample), the sample fixed sample length L_2 was 51 mm, which gives a fixing efficiency of 97%. When the sample with the temporary shape was reheated to 60 °C by reimmersing it in hot water, the length recovered to L_3 = 28 mm, which gives a recovery efficiency of 76%. Note that the time for the sample to recover, shown in Figure 11, was of the order of 30 min, which is very slow and may not be particularly useful for many shape memory applications. Although the driving force for shape memory behavior is rubber elasticity, i.e., the elastic restoring force that is stored in the network chains when the network is deformed, the kinetics of the recovery are influenced by the viscous properties of the polymer melt. In this case, the recovery experiment was carried out at 60 °C, where according to the data in Figures 8 and 9 the properties of the polymer were close to that of a critical gel. Thus, one might expect very slow relaxation behavior.

The reproducibility of the shape memory behavior was evaluated by cycling the shape memory test using the DMA with a tensile film fixture in the controlled force mode. The first cycle of the shape memory test of ZnCTBPSVP-1:1 is shown in Figure 12. The film sample was stretched to a strain of ε_{11} =

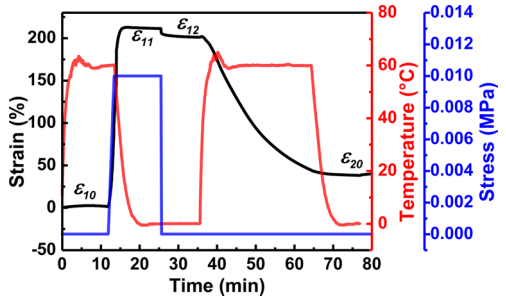

Figure 12. First cycle of the shape memory test of ZnCTBPSVP-1:1. ε_{10}: original strain of sample; ε_{11}: strain after stretching and cooling under load; ε_{12}: strain of fixed temporary shape after removing stress; and ε_{20}: recovered strain of the first cycle.

212% at 60 °C with a stress of 0.01 MPa and cooled to 0 °C, and then the stress was unloaded. After removing the stress, the sample contracted a bit, and the strain of the fixed temporary shape was ε_{12} = 201%. When the sample in the temporary shape was reheated to 60 °C, the strain recovered to 38%. The shape fixing efficiency, R_{1f}, and shape recovery efficiency, R_{1r}, were 95% and 81%, respectively.

Eight consecutive shape memory cycles for ZnCTBPSVP-1:1 are shown in Figure 13. The results for the first cycle, the one shown in Figure 12, were not as good as for the next seven cycles, which is a commonly observed result that is believed to be a consequence of some hysteresis due to the thermal

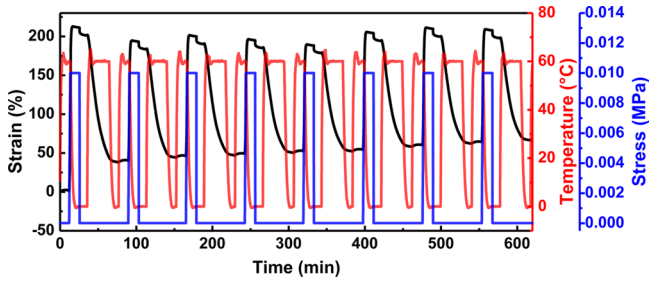

Figure 13. Eight consecutive shape memory cycles for ZnCTBPSVP-1:1.

DOI: 10.1021/acs.macromol.6b01785
Macromolecules 2016, 49, 7322−7330

mechanical history of the molding process. However, after the first cycle, the shape memory behavior was very reproducible with an average of the fixing efficiency. The figure reveals that the elastomer possesses a steady cycling shape memory property. The reproducibility of shape fixing efficiency for the last seven cycles was very good, and its average was 93% ± 0.7%. The average shape recovery efficiency of the last seven cycles was 97% ± 1%.

Note that the first cycle is also shown in Figure 13.

Note that the choice of 60 °C as the deformation temperature was arbitrary. The DSC analysis described earlier in the paper indicated that the two T_gs for ZnCTBPSVP-1:1 were −77 °C for the continuous, elastomer phase and 77 °C for the hard PSVP phase that provides the "permanent cross-links" for this SMP. Thus, any temperature between −77 and 77 °C may be used, in principle, for programming a temporary shape and recovering the permanent shape. That large temperature window provides excellent design possibilities.

In addition, the sample process large deformation ability under a relatively small stress under 60 °C and would not flow due to the pinning effect of nanodomains of the PSVP phase. However, the nanodomains of the PSVP phase which are taken as the cross-links in our work begin to soften at 18 °C according to the DMA data. So, the question is how could this elastomer show such good shape memory properties when we used a programming temperature of 60 °C? The point that needs to be brought out is that the permanent network is due to cross-linking the PSVP domains with the ZnCTB molecules, and the ion−metal bond persists to higher temperatures than the T_g of the PSVP domains. And, although the PSVP chains have more mobility than they did below T_g, that phase is probably still more viscous than the continuous CTB phase (which by itself is a lower viscosity liquid at those temperatures) such that there is no incentive for the PSVP chains to pull out of the domains, which would break the cross-links. So, above the T_g of the PSVP, the microstructure is actually a soft domain cross-linking a much lower viscosity liquid. Thus, the explanation is in part that although the PSVP domains soften, the supramolecular bonds are stable to much higher temperatures. So, the cross-link is still intact at 60 °C, although it is much softer than it was at lower temperature. But, still a PSVP chain pays a large enthalpic penalty to pull out of the domain and move through the CTB continuous phase. So, for the programming procedure used (i.e., short time at 60 °C) the PSVP chains do not flow; as a result, we can get decent shape memory. This is similar to an SBS block copolymer. Even though the PS T_g is 100 °C (actually less), the material does not easily flow until you get to much higher temperatures.[49] So, because thermodynamics favors the phase separation, flow does not occur until you provide more energy to the domains than you do at the glass transition.

CONCLUSIONS

A supramolecular shape memory elastomer was designed and synthesized using a blend of functionalized polybutadiene oligomers and functionalized poly(styrene-*co*-vinylpyridine) where a physically cross-linked network was produced by a transition metal complex between Zn^{2+} ions from carboxylated telechelic polybutadiene and the pyridine group of the PSVP. The microstructure of the elastomeric blend consisted of microphase-separated glassy nanodomains of principally PSVP, which served as cross-link junctions that were connected with polybutadiene chains. Thus, the intermolecular metal−pyridine complex most likely resided at the interface between the nanodomains and the soft rubber phase. The elastomer had reasonably good mechanical properties and was thermoplastic. Shape memory was achieved by tuning the intermolecular complex and using the microphase separation as a permanent network. The shape memory elastomer exhibited good shape memory properties for large deformations. For example, for a strain of 213%, the shape fixing and recovery efficiencies were as high as 95% and 81%, respectively, for the first shape memory cycle and were 93 ± 0.7% and 97 ± 1%, respectively, in the following seven cycles.

AUTHOR INFORMATION

Corresponding Authors

*E-mail: rweiss@uakron.edu (R.A.W.).
*E-mail: lengjs@hit.edu.cn (J.L.).
*E-mail: yj_liu@hit.edu.cn (Y.L.).

Notes

The authors declare no competing financial interest.

ACKNOWLEDGMENTS

The authors thank Dr. Kevin Cavicchi for fruitful discussions and suggestions about the polymer synthesis. F.X. thanks the Chinese Scholarship Council (CSC) for supporting her research at the University of Akron. This research was also partially supported by the Civil, Mechanical and Manufacturing Innovation (CMMI) Division within the Engineering Directorate of the National Science Foundation (Grant CMI-1300212). Special thanks to the University of Akron and Harbin Institute of Technology.

REFERENCES

(1) Leng, J.; Lan, X.; Liu, Y.; Du, S. Shape-memory polymers and their composites: Stimulus methods and applications. *Prog. Mater. Sci.* **2011**, *56* (7), 1077−1135.

(2) Wang, W.; Liu, Y.; Leng, J. Recent developments in shape memory polymer nanocomposites: Actuation methods and mechanisms. *Coord. Chem. Rev.* **2016**, *320*−*321*, 38−52.

(3) Berg, G. J.; McBride, M. K.; Wang, C.; Bowman, C. N. New directions in the chemistry of shape memory polymers. *Polymer* **2014**, *55* (23), 5849−5872.

(4) Ota, S. Current status of irradiated heat-shrinkable tubing in Japan. *Radiat. Phys. Chem.* **1981**, *18* (1−2), 81−87.

(5) Hu, J.; Chen, S. A review of actively moving polymers in textile applications. *J. Mater. Chem.* **2010**, *20* (17), 3346−3355.

(6) Lendlein, A.; Langer, R. Biodegradable, elastic shape-memory polymers for potential biomedical applications. *Science* **2002**, *296* (5573), 1673−1676.

(7) Xie, T.; Xiao, X.; Li, J.; Wang, R. Encoding localized strain history through wrinkle based structural colors. *Adv. Mater.* **2010**, *22* (39), 4390−4394.

(8) Pretsch, T.; Ecker, M.; Schildhauer, M.; Maskos, M. Switchable information carriers based on shape memory polymer. *J. Mater. Chem.* **2012**, *22* (16), 7757−7766.

(9) Du, H.; Liu, L.; Leng, J.; Peng, H.; Scarpa, F.; Liu, Y. Shape memory polymer S-shaped mandrel for composite air duct manufacturing. *Composite Structures* **2015**, *133*, 930−938.

(10) Liu, Y.; Du, H.; Liu, L.; Leng, J. Shape memory polymers and their composites in aerospace applications: A review. *Smart Mater. Struct.* **2014**, *23* (2), 023001.

(11) Reed, J. L., Jr.; Hemmelgarn, C. D.; Pelley, B. M.; Havens, E. In *Adaptive Wing Structures, Smart Structures and Materials 2005 - Industrial and Commercial Applications of Smart Structures Technologies*; White, E. V., Ed.; SPIE: San Diego, CA, 2005; pp 132−142.

DOI: 10.1021/acs.macromol.6b01785
Macromolecules 2016, 49, 7322−7330

(12) Lan, X.; Liu, Y.; Lv, H.; Wang, X.; Leng, J.; Du, S. Fiber reinforced shape-memory polymer composite and its application in a deployable hinge. *Smart Mater. Struct.* **2009**, *18* (2), 024002.
(13) Zhang, J.; Niu, Y.; Huang, C.; Xiao, L.; Chen, Z.; Yang, K.; Wang, Y. Self-healable and recyclable triple-shape PPDO-PTMEG co-network constructed through thermoreversible Diels-Alder reaction. *Polym. Chem.* **2012**, *3* (6), 1390−1393.
(14) Rivero, G.; Nguyen, L. T.; Hillewaere, X. K. D.; Du Prez, F. E. One-pot thermo-remendable shape memory polyurethanes. *Macromolecules* **2014**, *47* (6), 2010−2018.
(15) Guo, M.; Pitet, L. M.; Wyss, H. M.; Vos, M.; Dankers, P. Y. W.; Meijer, E. W. Tough stimuli-responsive supramolecular hydrogels with hydrogen-bonding network junctions. *J. Am. Chem. Soc.* **2014**, *136* (19), 6969−6977.
(16) Chen, S.; Yuan, H.; Chen, S.; Yang, H.; Ge, Z.; Zhuo, H.; Liu, J. Development of supramolecular liquid-crystalline polyurethane complexes exhibiting triple-shape functionality using a one-step programming process. *J. Mater. Chem. A* **2014**, *2* (26), 10169−10181.
(17) Weiss, R. A.; Izzo, E.; Mandelbaum, S. New design of shape memory polymers: Mixtures of an elastomeric ionomer and low molar mass fatty acids and their salts. *Macromolecules* **2008**, *41* (9), 2978−2980.
(18) Dong, J.; Weiss, R. A. Effect of crosslinking on shape-memory behavior of zinc stearate/ionomer compounds. *Macromol. Chem. Phys.* **2013**, *214* (11), 1238−1246.
(19) Zhang, L.; Brostowitz, N. R.; Cavicchi, K. A.; Weiss, R. A. Perspective: ionomer research and applications. *Macromol. React. Eng.* **2014**, *8* (2), 81−99.
(20) Hao, J. K.; Weiss, R. A. Mechanically tough, thermally activated shape memory hydrogels. *ACS Macro Lett.* **2013**, *2* (1), 86−89.
(21) Whittell, G. R.; Hager, M. D.; Schubert, U. S.; Manners, I. Functional soft materials from metallopolymers and metallosupramolecular polymers. *Nat. Mater.* **2011**, *10* (3), 176−88.
(22) Wu, X.; Xu, N.; Zhu, Z.; Cai, Y.; Zhao, Y.; Wang, D. Subcomponent self-assembly of polymer chains based on dynamic and geometrical coordination diversity of the first row transition metal ions. *Polym. Chem.* **2014**, *5* (4), 1202−1209.
(23) Kumpfer, J. R.; Rowan, S. J. Thermo-, photo-, and chemo-responsive shape-memory properties from photo-cross-linked metallosupramolecular polymers. *J. Am. Chem. Soc.* **2011**, *133* (32), 12866−74.
(24) Wang, Z.; Fan, W.; Tong, R.; Lu, X.; Xia, H. Thermal-healable and shape memory metallosupramolecular poly(n-butyl acrylate-co-methyl methacrylate) materials. *RSC Adv.* **2014**, *4* (49), 25486−25493.
(25) Noro, S. i.; Kitagawa, S.; Akutagawa, T.; Nakamura, T. Coordination polymers constructed from transition metal ions and organic N-containing heterocyclic ligands: Crystal structures and microporous properties. *Prog. Polym. Sci.* **2009**, *34* (3), 240−279.
(26) McCurdie, M. P.; Belfiore, L. A. Spectroscopic analysis of transition-metal coordination complexes based on poly(4-vinylpyridine) and dichlorotricarbonylruthenium(II). *Polymer* **1999**, *40* (11), 2889−2902.
(27) Belfiore, L. A.; Pires, A. T. N.; Wang, Y.; Graham, H.; Ueda, E. Transition-metal coordination in polymer blends and model systems. *Macromolecules* **1992**, *25* (5), 1411−1419.
(28) Weiss, R. A.; Sasongko, S.; Jerome, R. Graft copolymers of polystyrene and polyisoprene prepared by complexation of functionalized homopolymers. *Macromolecules* **1991**, *24* (9), 2271−2277.
(29) Zhang, L. H.; Kucera, L. R.; Ummadisetty, S.; Nykaza, J. R.; Elabd, Y. A.; Storey, R. F.; Cavicchi, K. A.; Weiss, R. A. Supramolecular multiblock polystyrene-polyisobutylene copolymers via ionic interactions. *Macromolecules* **2014**, *47* (13), 4387−4396.
(30) Sen, A.; Weiss, R. A.; Garton, A. Grafted-block copolymer networks formed by transition metal coordination of styrene- and butadiene-based polymers. In *Multiphase Polymers: Blends and Ionomers*; Utracki, L. A., Weiss, R. A., Eds.; ACS Symposium Series; American Chemical Society: Washington, DC, 1989; Vol. *395*, pp 353−369.
(31) Register, R. A.; Sen, A.; Weiss, R. A.; Li, C.; Cooper, S. L. Morphology and cation local structure in a blend of copper-neutralized carboxy-terminated polybutadiene and poly(styrene-co-4-vinylpyridine). *J. Polym. Sci., Part B: Polym. Phys.* **1989**, *27* (9), 1911−1925.
(32) Zhao, H.; Liu, S.; Jiang, M.; Yuan, X. f.; An, Y.; Liu, L. Micelle-like particles formed by carboxylic acid-terminated polystyrene and poly(4-vinyl pyridine) in chloroform/methanol mixed solution. *Polymer* **2000**, *41* (7), 2705−2709.
(33) Brostowitz, N. R.; Weiss, R. A.; Cavicchi, K. A. Facile fabrication of a shape memory polymer by swelling cross-linked natural rubber with stearic acid. *ACS Macro Lett.* **2014**, *3* (4), 374−377.
(34) Wu, K. H.; Wang, Y. R.; Hwu, W. H. FTIR and TGA studies of poly(4-vinylpyridine-co-divinylbenzene)−Cu(II) complex. *Polym. Degrad. Stab.* **2003**, *79* (2), 195−200.
(35) Ruokolainen, J.; Tanner, J.; ten Brinke, G.; Ikkala, O.; Torkkeli, M.; Serimaa, R. Poly(4-vinyl pyridine)/zinc dodecyl benzene sulfonate mesomorphic state due to coordination complexation. *Macromolecules* **1995**, *28* (23), 7779−7784.
(36) Fernandez-Berridi, M. J.; Iruin, J. J.; Irusta, L.; Mercero, J. M.; Ugalde, J. M. Hydrogen-bonding interactions between formic acid and pyridine. *J. Phys. Chem. A* **2002**, *106* (16), 4187−4191.
(37) Rodgers, M. T.; Stanley, J. R.; Amunugama, R. Periodic trends in the binding of metal ions to pyridine studied by threshold collision-induced dissociation and density functional theory. *J. Am. Chem. Soc.* **2000**, *122* (44), 10969−10978.
(38) Alcoutlabi, M.; McKenna, G. B. Effects of confinement on material behaviour at the nanometre size scale. *J. Phys.: Condens. Matter* **2005**, *17* (15), R461.
(39) Jackson, C. L.; McKenna, G. B. The glass transition of organic liquids confined to small pores. *J. Non-Cryst. Solids* **1991**, *131*, 221−224.
(40) Robertson, C. G.; Hogan, T. E.; Rackaitis, M.; Puskas, J. E.; Wang, X. Effect of nanoscale confinement on glass transition of polystyrene domains from self-assembly of block copolymers. *J. Chem. Phys.* **2010**, *132* (10), 104904.
(41) Williams, C. E.; Russell, T. P.; Jerome, R.; Horrion, J. Ionic aggregation in model ionomers. *Macromolecules* **1986**, *19* (11), 2877−2884.
(42) Lu, X.; Weiss, R. A. Specific interactions and ionic aggregation in miscible blends of nylon-6 and zinc sulfonated polystyrene ionomer. *Macromolecules* **1992**, *25* (23), 6185−6189.
(43) Einstein, A. Eine neue bestimmung der moleküldimensionen. *Ann. Phys.* **1906**, *324* (2), 289−306.
(44) Winter, H. H.; Mours, M. Rheology of polymers near liquid-solid transitions. *Adv. Polym. Sci.* **1997**, *134*, 165−234.
(45) Flory, P. J.; Rehner, J. Statistical mechanics of cross-linked polymer networks I. rubberlike elasticity. *J. Chem. Phys.* **1943**, *11* (11), 512−520.
(46) Tabsan, N.; Suchiva, K.; Wirasate, S. Effect of montmorillonite on abrasion resistance of SiO_2-filled polybutadiene. *Compos. Interfaces* **2012**, *19* (1), 1−13.
(47) Kim, M.-S.; Kim, D.-W.; Ray Chowdhury, S.; Kim, G.-H. Melt-compounded butadiene rubber nanocomposites with improved mechanical properties and abrasion resistance. *J. Appl. Polym. Sci.* **2006**, *102* (3), 2062−2066.
(48) https://www.matbase.com.
(49) Ji, S.; Hoye, T. R.; Macosko, C. W. Diamino telechelic polybutadienes for solventless styrene−butadiene−styrene (SBS) triblock copolymer formation. *Polymer* **2008**, *49* (24), 5307−5313.

DOI: 10.1021/acs.macromol.6b01785
Macromolecules 2016, 49, 7322−7330